J. Fluid Mech. (1986), *vol.* 164, *pp.* 91–105
Printed in Great Britain

Nonlinear interactions between convection, rotation and flows with vertical shear

By DAVID H. HATHAWAY
Space Science Laboratory, NASA/Marshall Space Flight Center, Huntsville, AL 35812

AND RICHARD C. J. SOMERVILLE
Scripps Institution of Oceanography, University of California, San Diego, La Jolla, CA 92093

(Received 20 December 1984 and in revised form 17 July 1985)

A three-dimensional and time-dependent numerical model is used to study the nonlinear interactions between thermal convective motions, rotation, and imposed flows with vertical shear. All cases have Rayleigh numbers of 10^4 and Prandtl numbers of 1.0. Rotating cases have Taylor numbers of 10^4.

For the non-rotating cases, the effects of the shear on the convection produce longitudinal rolls aligned with the shear flow and a downgradient flux of momentum. The interaction between the convection and the shear flow decreases the shear in the interior of the fluid layer while adding kinetic energy to the convective motions. For unit Prandtl number the dimensionless flux of momentum is equal to the dimensionless flux of heat.

For rotating cases with vertical rotation vectors, the shear flow favours rolls aligned with the shear and produces a downgradient flux of momentum. However, the Coriolis force turns the flow induced by the convection to produce a more complicated shear that changes direction with height. As in the non-rotating cases, the convective motions become more energetic by extracting energy from the mean flow. For Richardson numbers larger than about -1.0, the dominant source of eddy kinetic energy is the shear flow rather than buoyancy.

For rotating cases with tilted rotation vectors the results depend upon the direction of the shear. For weak shear, convective rolls aligned with the rotation vector are favoured. When the shear flow is directed to the east along the top, the rolls become broader and the convection weaker. For large shear in this direction, the convective motions are quenched by the competition between the shear flow and the tilted rotation vector. When the shear flow is directed to the west along the top, strong shear produces rolls aligned with the shear. The heat and momentum fluxes become large and can exceed those found in the absence of a tilted rotation vector. Countergradient fluxes of momentum can also be produced.

1. Introduction

Observations of the sun and the giant planets show vigorous thermal convection together with zonal flows which vary strongly with depth and latitude. We have only a limited understanding of the possible interactions between convection and such zonal flows with shear in rotating atmospheres. The few cases that have been studied suggest several mechanisms through which thermal convection may be important in driving zonal mean flows (e.g. Busse 1982, 1983; Hathaway & Somerville 1983). In view of the relatively undeveloped state of the subject, it seems worthwhile to

examine these phenomena further in highly idealized contexts before attempting more realistic simulations of solar or planetary atmospheres.

A substantial amount of work on convection in shear flows has been motivated by observations of cloud streets in the Earth's atmosphere (Brunt 1951; Kuettner 1971; LeMone 1973, 1983). Stability analysis (Kuo 1963; Deardorff 1965; Ingersoll 1966) and numerical simulations (Lipps 1971) indicate that flows with vertical shear produce longitudinal convective rolls by inhibiting the onset of convective rolls oriented transverse to the flow. Laboratory experiments by Hart (1971) and theoretical work by Clever & Busse (1977) and Clever, Busse & Kelly (1977) have shown how these rolls became wavy and eventually three-dimensional as the layer becomes more supercritical. Of these studies only LeMone (1973, 1983) has considered the effects due to rotation. Although she recognizes the possible importance of the tilted rotation vector in the tropics, her analysis of the momentum transport indicates that mesoscale pressure gradients dominate.

This paper reports the results of three-dimensional and time-dependent numerical simulation of thermal convection driven by heating from below, imbedded in a prescribed zonal flow with vertical shear and subject to rotation about an axis tilted from the vertical. We emphasize that the purpose of these exploratory integrations is to study a set of physical processes in isolation, not to mimic the properties of a realistic geophysical or astrophysical situation. Thus we have adopted the traditional assumptions of laboratory convection, such as considering a Boussinesq fluid of constant viscosity and conductivity, confined in plane parallel geometry between isothermal, rigid, no-slip boundaries. All of these assumptions are violated in real stellar and planetary atmospheres, and should be relaxed in future work.

In a previous paper (Hathaway & Somerville 1983, hereinafter referred to as Paper 1) we found an unexpected richness in the behaviour of convection in the presence of a tilted rotation vector. When the rotation vector is tilted from the vertical, the convection tends to become organized into a series of rolls whose axes are oriented north–south, i.e. parallel to the rotation axis. The Coriolis force acting on these convective motions drives a downward flux of eastward momentum. We found that this downward flux produces a mean flow which is directed to the east in the lower half of the layer and to the west in the upper half. In the absence of rotation a shear flow such as this would favour rolls whose axes are oriented east–west, i.e. parallel to the mean flow (e.g. Kuo 1963; Ingersoll 1966; Lipps 1971). In fact, a series of east–west rolls would produce an even stronger shear because such rolls cannot produce pressure gradients to balance the Coriolis force. Nevertheless, the constraint due to rotation prevails and produces north–south rolls, even though the positive feedback due to the shear would favour east–west rolls.

In Paper 1 the shear flow was produced by the effects of rotation on the convection itself. Such shear flows might also be produced in other contexts through a variety of other mechanisms. For example, horizontal temperature gradients in a rotating fluid can produce thermal wind shears in which the thermally induced horizontal pressure gradients are balanced by the Coriolis force on the mean wind. In slowly rotating atmospheres pressure gradients can lead directly to shear flows. External stresses at the upper and lower boundaries of a layer are another means of generating a mean flow with a vertical shear. Shear flows might also be produced by Reynolds stresses or Coriolis forcing on a larger scale of convective motions or a meridional circulation. In the study reported here we examine the effects of a mean flow with vertical shear on the convective motions in a rotating layer. The shear flow is externally imposed by moving the rigid upper and lower boundaries in opposite

directions and introducing a lateral force which opposes the Coriolis force on the shear. In this manner we can impose arbitrary shears to investigate the interactions with the convective motions.

2. The model

We have chosen a highly idealized system for study and have modelled it using the full nonlinear Boussinesq equations. Our representation of the influence of rotation is quite general, in that we have retained all of the Coriolis terms rather than making *a priori* assumptions concerning their relative magnitudes. The layer of fluid is positioned tangentially to a rotating sphere at a latitude ϕ. We neglect the effects of curvature but include both the vertical and horizontal components of the rotation vector to simulate convection at various latitudes. We use rigid (non-slip) top and bottom boundaries and periodic side boundaries to represent an infinite plane parallel layer.

The numerical procedure used is an efficient finite-difference technique described by Somerville & Gal-Chen (1979). The computational domain is usually 1 unit in the z- (upward) direction by 10.0 units in the x- (eastward) direction by 10.0 units in the y- (northward) direction. For some of the cases studied the convection forms smaller cells, and so the domain was limited to dimensions of $1.0 \times 5.0 \times 5.0$. The calculations involve 57 600 grid points in an array with 25 points in z, 48 points in x and 48 points in y. One time step takes about 4 s on the CRAY 1 machines at the National Center for Atmospheric Research.

The vertical shear is imposed by sliding the upper boundary in one direction and the lower boundary in the opposite direction. In the absence of rotation this procedure produces a Couette flow with constant vertical shear. However, in order to maintain a constant shear in the presence of rotation we must introduce an imposed force transverse to the mean flow which balances the Coriolis force. This imposed force, together with the vertical pressure gradient due to hydrostatics and the vertical component of the Coriolis force acting on the imposed flow, can then be removed from the equations for the convection. The pressure in this basic state is given by

$$\frac{1}{\rho_0}\frac{\mathrm{d}p_0}{\mathrm{d}z} = -(1-\alpha T_0)g + 2\Omega\cos\phi\, U_0, \tag{2.1}$$

where p_0 is the pressure, ρ_0 the density, T_0 the temperature, U_0 the imposed velocity, α the volumetric coefficient of expansion, g the acceleration due to gravity and Ω the rotation frequency. The imposed force in the basic state is given by

$$F_y = 2\Omega\sin\phi\, U_0. \tag{2.2}$$

The quantities are made dimensionless by using D, the depth of the layer, as the unit of length, D^2/ν, the viscous time scale, as the unit of time, and ΔT, the imposed temperature difference across the layer, as the unit of temperature. The dimensionless equations that govern the convective motions are given by the mass continuity equation

$$\frac{\partial u}{\partial x}+\frac{\partial v}{\partial y}+\frac{\partial w}{\partial z} = 0, \tag{2.3}$$

the three components of the momentum equation

$$\frac{\partial u}{\partial t}+(u+U_0)\frac{\partial u}{\partial x}+v\frac{\partial u}{\partial y}+w\frac{\partial}{\partial z}(u+U_0)-Ta^{\frac{1}{2}}\sin\phi v+Ta^{\frac{1}{2}}\cos\phi w = -\frac{\partial p}{\partial x}+\nabla^2 u, \tag{2.4}$$

$$\frac{\partial v}{\partial t}+(u+U_0)\frac{\partial v}{\partial x}+v\frac{\partial v}{\partial y}+w\frac{\partial v}{\partial z}+Ta^{\frac{1}{2}}\sin\phi u=-\frac{\partial p}{\partial y}+\nabla^2 v, \tag{2.5}$$

$$\frac{\partial w}{\partial t}+(u+U_0)\frac{\partial w}{\partial x}+v\frac{\partial w}{\partial y}+w\frac{\partial w}{\partial z}-Ta^{\frac{1}{2}}\cos\phi u=-\frac{\partial p}{\partial z}+\frac{Ra}{Pr}\Theta+\nabla^2 w, \tag{2.6}$$

and the thermal-energy equation

$$\frac{\partial \Theta}{\partial t}+(u+U_0)\frac{\partial \Theta}{\partial x}+v\frac{\partial \Theta}{\partial y}+w\frac{\partial}{\partial z}(\Theta+T_0)=\frac{1}{Pr}\nabla^2\Theta, \tag{2.7}$$

where the Taylor number is
$$Ta=\frac{4\Omega^2 D^4}{\nu^2} \tag{2.8}$$

the Rayleigh number is
$$Ra=\frac{\alpha g\,\Delta T\,D^3}{\kappa\nu} \tag{2.9}$$

and the Prandtl number is
$$Pr=\frac{\nu}{\kappa}. \tag{2.10}$$

The imposed shear is in the x-direction and is given by

$$U_0=Re\,(z-\tfrac{1}{2}), \tag{2.11}$$

where
$$Re=\frac{D\,\Delta U}{\nu} \tag{2.12}$$

is the Reynolds number. Here ν is the kinematic viscosity, κ is the thermal diffusivity and ΔU is the imposed velocity difference across the layer. In addition to these imposed parameters we calculate the Richardson number

$$Ri=-\frac{\alpha g\,\Delta T\,D}{(\Delta U)^2}=-\frac{Ra}{Pr\,Re^2} \tag{2.13}$$

for each case. The Richardson number gives a measure of the ratio of the timescales for the shear and for buoyancy and serves as a useful measure of the relative importance of these two sources of energy.

3. Diagnostic equations

In analysing the results from our calculations we consider the balance equations for the momentum and energy in the layer. If we define a horizontally averaged quantity as

$$\bar{a}(z)=\frac{1}{L_x L_y}\int_0^{L_y}\int_0^{L_x} a(x,y,z)\,\mathrm{d}x\,\mathrm{d}y, \tag{3.1}$$

then the mean flow is given by

$$U(z)=U_0(z)+\bar{u}(z) \tag{3.2}$$

and
$$V(z)=\bar{v}(z). \tag{3.3}$$

To calculate the momentum balance we take the horizontal average of the two horizontal components of the momentum equation. This gives

$$\frac{\partial \bar{u}}{\partial t}=-\frac{\mathrm{d}}{\mathrm{d}z}\overline{uw}+Ta^{\frac{1}{2}}\sin\phi\,\bar{v}+\frac{\mathrm{d}^2\bar{u}}{\mathrm{d}z^2} \tag{3.4}$$

and
$$\frac{\partial \bar{v}}{\partial t} = -\frac{\mathrm{d}}{\mathrm{d}z}\overline{vw} - Ta^{\frac{1}{2}} \sin\phi \bar{u} + \frac{\mathrm{d}^2 \bar{v}}{\mathrm{d}z^2}. \tag{3.5}$$

We then define a normalized momentum flux vector $\boldsymbol{M}$ with components

$$M_x = \frac{1}{Re}\left[\frac{\mathrm{d}U}{\mathrm{d}z} - \overline{uw}\right] \tag{3.6}$$

and
$$M_y = \frac{1}{Re}\left[\frac{\mathrm{d}V}{\mathrm{d}z} - \overline{vw}\right]. \tag{3.7}$$

These fluxes need not be constant with depth. For steady-state flows we find

$$\frac{\mathrm{d}M_x}{\mathrm{d}z} = -Ta^{\frac{1}{2}} \sin\phi \bar{v} \tag{3.8}$$

and
$$\frac{\mathrm{d}M_y}{\mathrm{d}z} = +Ta^{\frac{1}{2}} \sin\phi \bar{u}. \tag{3.9}$$

In the absence of rotation, $Ta = 0$, there is no divergence of these momentum fluxes within the layer itself and the momentum transport is characterized by a scalar 'momentum number'

$$Mo = M_x + M_y, \tag{3.10}$$

where $M_y = 0$ by symmetry.

To calculate the energy balance we take volume averages of the different energy components. We define a volume average for the layer by

$$\langle a \rangle = \int_0^1 \bar{a}(z)\,\mathrm{d}z. \tag{3.11}$$

The mean kinetic energy is then given by

$$\langle \bar{K} \rangle = \int_0^1 [\tfrac{1}{2}(U_0 + \bar{u})^2 + \tfrac{1}{2}\bar{v}^2]\,\mathrm{d}z, \tag{3.12}$$

the eddy kinetic energy is given by

$$\langle K' \rangle = \frac{1}{2}\int_0^1 [\overline{(u-\bar{u})(u-\bar{u})} + \overline{(v-\bar{v})(v-\bar{v})} + \overline{ww}]\,\mathrm{d}z \tag{3.13}$$

and the gravitational potential energy is given by

$$\langle P \rangle = -\frac{Ra}{Pr}\int_0^1 \bar{\Theta} z\,\mathrm{d}z. \tag{3.14}$$

Differentiating these quantities with respect to time then gives

$$\frac{\partial \langle K' \rangle}{\partial t} = C(\bar{K}, K') + C(P, K') - F1, \tag{3.15}$$

$$\frac{\partial \langle K \rangle}{\partial t} = -C(\bar{K}, K') + E - F2, \tag{3.16}$$

and
$$\frac{\partial \langle P \rangle}{\partial t} = -C(P, K') - D1, \tag{3.17}$$

where
$$C(\bar{K}, K') = -\int_0^1 \overline{uw}\frac{\mathrm{d}U}{\mathrm{d}z}\,\mathrm{d}z - \int_0^1 \overline{vw}\frac{\mathrm{d}V}{\mathrm{d}z}\,\mathrm{d}z \tag{3.18}$$

represents the conversion of mean kinetic energy into eddy kinetic energy through the eddy momentum fluxes, and

$$C(P, K') = \frac{Ra}{Pr}\langle w\Theta \rangle \tag{3.19}$$

represents the conversion of available potential energy into eddy kinetic energy through the heat flux. Both forms of kinetic energy are diminished by viscous losses given by

$$F1 = \langle \nabla u \cdot \nabla u + \nabla v \cdot \nabla v + \nabla w \cdot \nabla w \rangle \tag{3.20}$$

and

$$F2 = \int_0^1 \left[\left(\frac{d\bar{u}}{dz}\right)^2 + \left(\frac{d\bar{v}}{dz}\right)^2 - U_0 \frac{d^2\bar{u}}{dz^2} \right] dz. \tag{3.21}$$

Potential energy is lost by the thermal diffusion at the boundaries as given by

$$D1 = \frac{Ra}{Pr^2} \frac{d\bar{\Theta}}{dz}\bigg|_{z=1}. \tag{3.22}$$

The term

$$E = \int_0^1 V(z) F_y \, dz \tag{3.23}$$

represents a change in the mean kinetic energy due to work done against the imposed force F_y in the basic state. As noted earlier, this force can arise from several different mechanisms.

Another useful quantity for characterizing these flows is the dimensionless heat flux, given by the Nusselt number

$$Nu = 1 - \frac{1}{Pr} \frac{d\bar{\Theta}}{dz} + \overline{w\Theta}, \tag{3.24}$$

the ratio of the total heat flux to the flux that would be carried by conduction alone. For a steady state the Nusselt number is independent of depth.

In the following section we briefly review the earlier results for convection in rotating layers without imposed shears. In §5 we present results for convection in shear flows without rotation, while in §6 we include both rotation and shear flows.

4. Effects due to rotation

The effects on convection due to rotation about a vertical axis have been described by Veronis (1959), Chandrasekhar (1961), Weiss (1964), Somerville (1971) and Somerville & Lipps (1973). These effects were recently re-examined in Paper 1 and are reviewed here for reference.

For comparison with later cases, we ran the code for a non-rotating case with $Ra = 10000$ (about six times the critical Rayleigh number). As the flow evolves, adjacent cellular elements join to form structures whose horizontal scale is considerably larger than the rolls of approximately square cross-section produced by linear theory. At this Rayleigh number the flow is strongly nonlinear, with typical dimensionless velocities near 17, so that the fluid traverses the layer in less than a tenth of a diffusion time. The Nusselt number for this case is about 2.38.

To examine the effects due to rotation about a vertical axis, we ran a case with $Ra = 10000$ and $Ta = 10000$ at 90° latitude. Here the effects due to rotation are quite strong. The large cells initially present from the first run quickly decay and are replaced by smaller ones. This result is expected from linear-stability theory, which yields a horizontal scale that decreases with increasing rotation rate. Dissipative

processes exact a heavier toll on these smaller-scale motions. The typical dimensionless velocities in this case are about 10, nearly half those of the non-rotating case, and the Nusselt number is about 1.75. An elegant physical interpretation of this result was given by Veronis (1959), who showed that, as the Coriolis force induces a velocity component parallel to the roll axes, the motion tends to conserve its wavelength measured in the plane containing the streamlines. As the rotation rate increases, the angle between this plane and the roll boundaries becomes smaller and so the width of the rolls decreases.

The effects due to a tilted rotation vector, typical of low-latitude regions, have recently been determined from linear calculations by Hathaway, Toomre & Gilman (1980) and from the nonlinear simulations described in Paper 1. Keeping the rotation rate and thermal forcing the same as in the previous rotating case we then tilted the rotation vector to represent a latitude of 15°. The tilt of the rotation vector profoundly influences the structure of the convection. The convective elements take on a pronounced north–south orientation. A strong correlation between vertical and east–west motions is produced. This correlation is attributable to the horizontal component of the rotation vector and can induce substantial mean flows. For this case typical convective velocities are about 14 and the induced mean flow is directed toward the west–north–west in the upper half of the layer and to the east–south–east in the bottom half, with an amplitude of about 4. The Nusselt number for this case is about 1.95. In spite of the shear flow the convection is still dominated by the tilted rotation vector and forms a pattern of north–south rolls.

5. Effects due to shear

The effects on convection due to imposed shear flows have been described by Brunt (1951), Kuo (1963), Deardorff (1965), Ingersoll (1966), and Lipps (1971). Strong vertical shear flows tend to organize the convection into a series of rolls aligned with the mean flow. Velocity correlations are produced which tend to transport momentum down the gradient and decrease the energy in the mean flow. Although the convection can extract energy from the mean flow in this manner, theory and experiment show that the critical Rayleigh number is unchanged by the presence of the shear flow. For strong thermal forcing these rolls become three-dimensional. This transition from two-dimensional rolls to three-dimensional cells has been studied experimentally by Hart (1971) and theoretically by Clever & Busse (1977) and Clever, Busse & Kelly (1977).

We have run three non-rotating cases with imposed shear flows having Reynolds numbers of 50, 100 and 200. All three cases have $Ra = 10000$ and $Pr = 1.0$. As the imposed shear increases the Richardson number increases from -4.0 to -1.0 to -0.25. Each case was run for 1500 time steps, which typically represents about one unit of dimensionless time and is sufficiently long to allow the flow to evolve to a quasi-equilibrium state.

The final flow field for the first of these cases is shown on figure 1 (plate 1). The upper surface moves toward the east while the lower surface moves toward the west with a dimensionless velocity of 25. Colour is used to represent temperature, with yellow being hot and red being cold. The trajectories of 700 black markers are plotted to show the flow on the three visible surfaces. While there is a tendency to form convective rolls aligned with the shear, the convection for this case is more cellular in form and suggest a secondary instability of the rolls like those described by Clever & Busse (1977) and Clever, Busse & Kelly (1977).

Eastward momentum is transported downward in this case, producing a much weaker shear flow in the interior of the fluid. Although the Nusselt number for this case, $Nu = 2.34$, is slightly smaller than for the corresponding non-sheared case, described in Paper 1, the typical velocities are somewhat higher with r.m.s. values of about 19 in the dimensionless units. This is reflected in the larger horizontal velocities but smaller vertical velocities found in the flow field relative to the unsheared case. The momentum flux number Mo is 2.22, which suggests that even in this relatively weak shear flow the convection is fairly efficient in transporting momentum. The ratio of the energy-conversion rate ($C(\bar{K}, K'$) from the mean kinetic energy, to the conversion rate $C(P, K')$ from available potential energy is 0.10 for this case. This indicates that the dominant energy source for the convective flow is buoyancy rather than the shear flow.

The second case has $Re = 100$ or $Ri = -1.0$. The final flow field for this case is shown in figure 2 (plate 1). Here the convection forms broad rolls which are well aligned with the shear flow. The Nusselt number increases slightly over that for the previous case: here $Nu = 2.37$. The momentum flux increases more dramatically and so $Mo = 2.37$ and typical velocities are 25. The large downward flux of eastward momentum is quite evident in figure 2. The particle trajectories on the southern surface show that downward and eastward velocities are well correlated. This correlation is also apparent in the flow field seen on the upper surface – eastward flows are found in the cool, red downdraughts while westward flows are found in the hot, yellow updraughts. The ratio of the conversion rate from mean kinetic energy to the conversion rate from available potential energy is 0.39 for this case. Thus, with $Ri = -1.0$ the shear flow becomes an important source of energy for the convection.

The third non-rotating case has $Re = 200$ or $Ri = -0.25$. The final flow field for this case is shown in figure 3 (plate 1). Although the size and orientation of the convective rolls remains the same as in the previous case, changes can be seen in the magnitude of the horizontal flows. The Nusselt number for this case increases to $Nu = 2.44$, the momentum flux number increases to $Mo = 2.44$ and the typical velocities are 39. Here too the downward flux of eastward momentum is quite evident in the flow field shown in figure 3. The ratio of the energy conversion rates is 1.46 for this case, so with $Ri = -0.25$ the shear flow is the dominant source of eddy kinetic energy.

The mean flows for these three non-rotating cases are shown in figure 4. The solid lines represents the imposed flow while the dashed lines represent the mean flow in the presence of convection. The mean flow in the direction transverse to the imposed shear vanishes for these three cases, as would be expected from symmetry. The thickness of the shear boundary layers at the top and bottom of the layer is a measure of the momentum flux and decreases slightly as the imposed shear increases. We note that for this fluid, with $Pr = 1.0$, $Mo = Nu$ for those cases with strong shears, $Ri > -1$. The proportionality of these two quantities at high Rayleigh numbers was discussed by Ingersoll (1966). As defined here the proportionality becomes an equality for $Pr = 1.0$.

6. Combined effects of rotation and shear

Very few theoretical studies have been published on convection in the presence of both rotation and shear. Those that have been published, including Flasar & Gierasch (1978) and Hathaway, Toomre & Gilman (1980), have used thermal winds in which a north–south temperature gradient produces a wind shear in the presence of rotation.

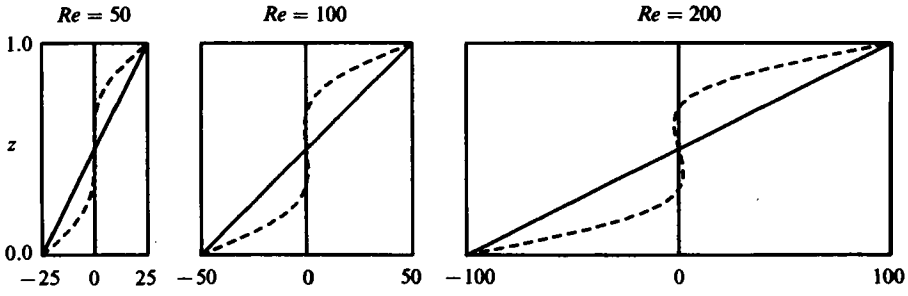

FIGURE 4. The mean flows for the three non-rotating cases. $Ra = 10000$, $Pr = 1.0$ and $Ta = 0$. Height above the bottom surface is plotted vertically while the mean flows are plotted in the horizontal direction. The imposed shear flow for each case is represented by the solid diagonal lines. The resultant zonal (west to east) flows are shown as dashed lines. For these cases the resultant flows are purely zonal with the shear concentrated in the boundary layers near the top and bottom surfaces.

We chose not to include a thermal wind in this study. Instead, the source of the shear is left unspecified to retain generality and to isolate the effects due to shear from the thermal effects due to north–south temperature gradients.

We have run nine cases with rotation and shear, all with $Ra = 10000$, $Pr = 1.0$ and $Ta = 10000$. The first three cases are for a latitude of 90° with $Re = 50$, 100 and 200. The next three are for a latitude of 15° with $Re = 50$, 100 and 200. Since there is a preferred horizontal direction in the low-latitude cases, we ran another set with the shear flow reversed in direction, thus $Re = -50$, -100 and -200.

The final flow field for the first of these cases at 90° is shown in figure 5 (plate 2). The shear tends to produce rolls which are nearly aligned with the mean flow although there appears to be some tendency to produce kinks in the rolls. The rolls are rather narrow, as they are in the absence of any shear, but the Nusselt number is somewhat larger, $Nu = 1.85$, than in the corresponding case without shear described in Paper 1. Although the time-averaged statistics for the flow are fairly stable they do fluctuate considerably, as does the convection pattern itself. During the last 500 time steps the depth-averaged Nusselt number varies from a minimum of 1.74 to a maximum of 2.09. The ratio of the energy-conversion rates for this case is about 0.32, with buoyancy being the dominant source of energy for the eddies. The depth-averaged momentum-flux number for this case is 2.27, but in the presence of rotation the momentum flux varies with height as indicated by (3.8) and (3.9). The y-component of this flux is only about 5% of the total. We also find that for this case the mean kinetic-energy losses to eddy kinetic energy $-C(\overline{K}, K')$ are nearly equal to the gain E due to work done by the imposed force, as defined in (3.23).

The flow field for the second case at 90°, with $Re = 100$, is shown in figure 6 (plate 2). Although the eddies are aligned with the flow the convection is not as well organized as in the more weakly sheared case. The Nusselt number increases slightly to $Nu = 1.86$ and the momentum flux increases to $Mo = 2.32$ with nearly 10% in the y-component. The ratio of energy-conversion rates increases dramatically to about 1.40, indicating that the shear dominates the eddy energetics. As in the previous case, the balance in the energetics of the mean flow has losses to the eddies nearly balanced by the gain due to the imposed force.

The flow field for the third case at 90°, with $Re = 200$, is shown in figure 7 (plate 2). Again the eddies are aligned with the shear but are more chaotic than in the two more weakly sheared cases. The Nusselt number for this case increases to $Nu = 2.35$,

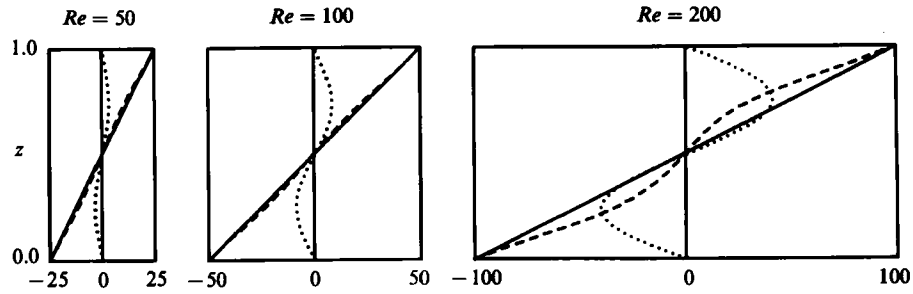

FIGURE 8. The mean flows for the three rotating cases at 90°. $Ra = 10000$, $Pr = 1.0$ and $Ta = 10000$. Except in the high-Reynolds-number case the mean zonal flow hardly changes from the imposed flow. The mean meridional flows, shown by the dotted lines, become very strong as the shear is increased. Except for the addition of these meridional flows, the format of this figure is the same as that of figure 4.

while the average momentum flux becomes $Mo = 5.16$ with slightly more than 10% in the y-component. The ratio of energy-conversion rates is 8.55, again indicating that the shear flow dominates the eddy energetics.

The mean flows for these three cases at 90° are shown in figure 8. In the first two cases the mean east–west flow, represented by the dashed line, is nearly equal to the imposed flow. However, all three cases also exhibit fairly strong north–south flows, represented by the dotted lines in the figure. For the third case the shear in the meridional flow exceeds that in the zonal flow. This meridional flow makes the mean flow direction change with depth. This may be the reason why the convection is less well organized in this case.

The next set of cases are for a latitude of 15°. The flow field for the first of these, with $Re = +50$, is shown in figure 9 (plate 3). Here the eddies tend to be aligned with the rotation axis instead of the shear. With $Nu = 1.88$ the heat flux is slightly smaller than for the unsheared case. For the average momentum flux we find $Mo = 1.50$ with about 15% in the y-component. The ratio of energy-conversion rates is about 0.08 so buoyancy dominates the eddy energetics.

The flow field for the next case, with $Re = +100$, is shown in figure 10 (plate 3). Again the eddies tend to be aligned with the rotation axis but they are much broader and less energetic. Lipps (1971) also found this behaviour for non-rotating layers when the convection is constrained to rolls aligned transverse to the shear. Here the Nusselt number drops dramatically to $Nu = 1.23$ and the momentum flux gives $Mo = 1.00$. The ratio of the energy-conversion rates decreases to 0.003 so that buoyancy is by far the most dominant source of eddy kinetic energy and very little momentum is transported by the eddies.

The flow field for the case with $Re = +200$ is shown in figure 11 (plate 3). After 500 time steps the convective motions are quenched! Both Nu and $Mo = 1.00$ and there is no conversion of energy from one form to another. This result is consistent with linear-stability theory (Hathaway, Toomre & Gilman 1980). The tilted rotation vector tends to stabilize rolls aligned with the shear. The shear tends to stabilize rolls aligned with the rotation vector. Together these effects stabilize all forms of convection.

The mean flows for these three cases are shown in figure 12. For $Re = +50$ the mean zonal flow is slightly weaker than the imposed flow and the meridional flow is extremely weak. For $Re = +100$ the mean zonal flow is essentially unchanged from

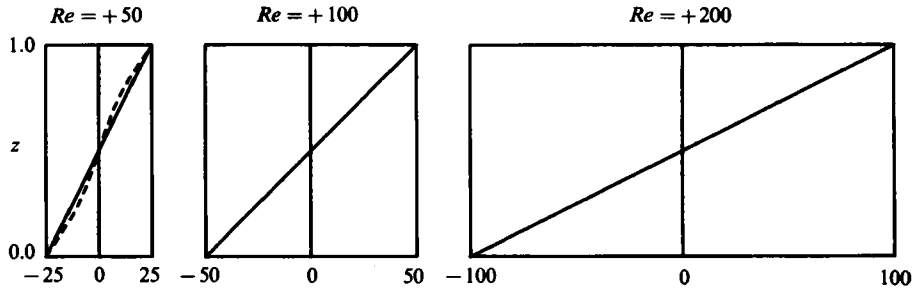

FIGURE 12. The mean flow fields for the rotating cases at 15° with positive shears imposed. $Ra = 10000$, $Pr = 1.0$ and $Ta = 10000$. The mean zonal flow is slightly changed from the imposed flow for $Re = 50$. For $Re = 100$ and 200 the mean zonal flow equals the imposed flow. In all three cases no meridional flows are produced.

the imposed flow and again the meridional flow is extremely weak. For $Re = +200$ only the imposed flow remains after the convective motions cease.

For the next three cases the mean-flow direction is reversed. The final flow field for the first case, with $Re = -50$, is shown in figure 13 (plate 4). Here too the eddies are aligned with the rotation vector. The heat flux gives $Nu = 1.89$, essentially the same as with $Re = +50$, but the average momentum flux gives $Mo = 0.50$, again with less than 10% in the y-component. For this case the convection actually assists in moving the top and bottom boundaries by producing a countergradient momentum flux! This is not unsuspected since we found in Paper 1 that the tilted rotation vector produces a mean flow in this sense. Eddy kinetic energy is converted into mean kinetic energy, so $C(\overline{K}, K')$ is negative. Of course, the magnitude of this conversion rate is still smaller than the production of eddy kinetic energy by buoyancy.

The flow field for the next case, with $Re = -100$, is shown in figure 14 (plate 4). Here the eddies are aligned with the shear instead of the rotation vector. The heat flux increases substantially, giving $Nu = 2.42$, and the eddy momentum flux changes sign to give $Mo = 1.14$. However, the conversion rate from mean kinetic energy is still only one tenth the rate due to buoyancy.

The flow field for the final case, with $Re = -200$, is shown in figure 15 (plate 4). For this case the convection forms rolls which are well aligned with the shear flow. The fluxes of both heat and momentum increase substantially to give $Nu = 3.05$ and $Mo = 2.57$ and the ratio of energy-conversion rates increases to 1.74, indicating that the shear flow dominates the eddy energetics. Here, as in most other cases, the y-component of the momentum flux is less than about 10% of the total.

The mean flows for these final three cases are shown in figure 16. For $Re = -50$ the mean zonal flow is enhanced and a small meridional flow is produced. For $Re = -100$ the mean zonal flow is slightly weaker than the imposed flow and the meridional flow, while also weak, has reversed direction from that in the weakly sheared case. For $Re = -200$ the mean zonal flow has much less shear than the imposed flow and the meridional flow is substantial.

The results of these calculations are summarized in table 1. In all cases we find that the contribution to $C(\overline{K}, K')$ from the second term in (3.18) is negligible and the y-component of the momentum flux is small. There is very little exchange of energy and momentum between the mean meridional flow and the convective eddies.

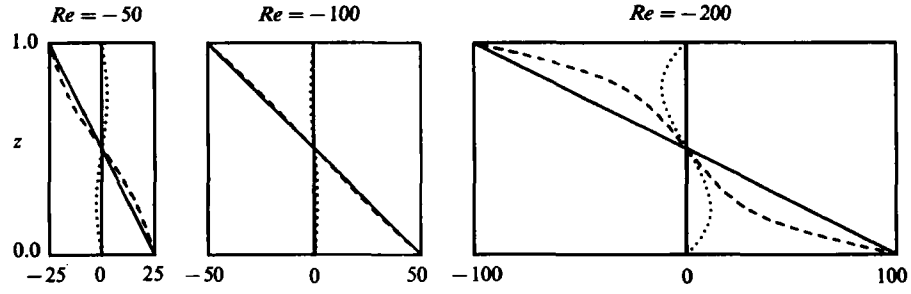

FIGURE 16. The mean flows for the three rotating cases at 15° with negative shears imposed. $Ra = 10000$, $Pr = 1.0$ and $Ta = 10000$. For $Re = -50$ the mean flow is stronger than the imposed flow and the meridional flow is directed to the north in the upper half of the layer. For $Re = -100$ the mean zonal flow is just slightly weaker than the imposed flow and the meridional flow is also weak but directed toward the south in the upper half of the layer. For $Re = -200$ the mean zonal flow is much weaker than the imposed flow and the meridional flow is quite strong and directed toward the south in the upper half of the layer.

Ta	ϕ	Re	Nu	Mo	$C(P, K')$	$C(\overline{K}, K')$	Figure
0	—	50	2.34	2.22	1.34×10^4	1.37×10^3	1
0	—	100	2.37	2.37	1.37×10^4	5.28×10^3	2
0	—	200	2.44	2.44	1.44×10^4	2.10×10^4	3
10^4	90°	50	1.85	2.27	8.55×10^3	2.72×10^3	5
10^4	90°	100	1.86	2.32	8.64×10^3	1.41×10^4	6
10^4	90°	200	2.35	5.16	1.35×10^4	1.15×10^5	7
10^4	15°	+50	1.88	1.50	8.80×10^3	6.88×10^2	9
10^4	15°	+100	1.23	1.00	2.30×10^3	6.30×10^0	10
10^4	15°	+200	1.00	1.00	0	0	11
10^4	15°	−50	1.89	0.50	8.90×10^3	-1.64×10^3	13
10^4	15°	−100	2.42	1.14	1.42×10^4	$+1.44 \times 10^3$	14
10^4	15°	−200	3.05	2.57	2.05×10^4	$+3.57 \times 10^4$	15

TABLE 1. Summary of results

7. Conclusions

Using a three-dimensional and time-dependent numerical model we have studied interactions between convection, rotation and vertical shear flows. In the absence of rotation the convective motions become dominated by the shear flow when the Richardson number (Ri) becomes greater than about -1.0. Both heat and momentum are carried down their respective gradients. The fluxes of heat and momentum, when normalized with respect to their values in the absence of convection, increase as the shear increases and are equal to each other in magnitude for these fluids with $Pr = 1.0$. Away from the top and bottom boundaries the convection tends to eliminate any gradients in the mean temperature and mean flow.

In the presence of both rotation and shear the behaviour of the convection is much more complicated and more interesting, especially when the rotation vector is tilted from the vertical. Rotation about a vertical axis turns the induced mean flow to a direction nearly orthogonal to the imposed flow. In addition, the convection itself also tends to enhance the cross-shear flow while extracting energy and momentum

from the imposed flow. The change in mean flow direction with height may be responsible for the more complicated convection patterns seen.

When the rotation vector is tilted from the vertical the behaviour of the convection depends upon the direction of the imposed shear. In Paper 1 we found that the horizontal component of the rotation vector tends to produce a zonal flow which is directed to the west in the upper half of the layer and to the east in the lower half. When the imposed flow is in the opposite direction (positive Reynolds numbers) the convective motions are less energetic and are even suppressed entirely when the shear is strong. When the imposed flow is in the same direction as that produced by the rotation the convective motions are enhanced and a countergradient flux of momentum can be produced. For these cases (with negative Reynolds numbers), the fluxes of heat and momentum can even exceed the values found in the non-rotating cases.

This type of behaviour was suggested by the linear-stability analysis of Hathaway, Toomre & Gilman (1980) for convection in a thermal wind shear. The wind shear stabilizes the transverse rolls while the tilted rotation vector stabilizes the longitudinal rolls. When both effects are strong the convective motions are quenched. The curious effect is the enhancement of the convection when the shear flow is reversed. Hathaway, Toomre & Gilman suggested that the source of the instability was the meridional tilt of the convective rolls. If the meridional motions are tilted such that energy is extracted from the mean kinetic energy and buoyancy is augmented by the horizontal temperature field then the convection could be enhanced. Here, however, there is no horizontal temperature gradient and the convective motions shown in figures 14 and 15 do not show any substantial tilt in the meridional motions.

The countergradient flux of momentum for the case with $Re = -50$ is also noteworthy. LeMone (1983) found a similar flux for a line of cumulonimbus observed during GATE. Her analysis suggests that this observed flux was due to a mesoscale pressure field and not the horizontal component of the rotation vector. Yet the tilted rotation vector quite naturally produces this countergradient flux. The Coriolis force turns upflows to the west and downflows to the east to give a *downward* flux of eastward momentum. LeMone (1983) notes that the Coriolis force can also turn eastward flows up and westward flows down to produce an *upward* flux of eastward momentum. Since the horizontal flows were stronger than the vertical flows she concludes that the Coriolis force is not responsible for the observed countergradient flux. However, for longitudinal rolls oriented east–west the Coriolis force on vertical flows cannot be balanced by (horizontal) pressure gradients since none can be produced in that direction. However, (vertical) pressure gradients can balance the Coriolis force on the horizontal flows. In cases studied here, and in Paper 1, the net result is a downward flux of eastward momentum which gives a net countergradient momentum flux when $Re = -50$.

Further implications of this work for geophysical and astrophysical flows will depend upon the actual circumstances involved in producing the shear flow. If the shear is produced by a horizontal temperature gradient then the horizontal heat flux would have to be considered. For the non-rotating cases it would be interesting to study fluids with different Prandtl numbers to determine how heat and momentum are transported by convection. For rotating objects, such as the sun and the giant planets, the shear flows may substantially alter the outward flow of heat. Larger fluxes would be expected where the zonal velocity decreases with depth.

The attempt to explain convective phenomena in the Earth's atmosphere in terms of Rayleigh–Bénard convection has a long history (Agee 1984). For tropical convection on Earth the importance of rotation, among many uncertainties, is not yet

well understood. It would be premature to draw firm conclusions about the effects of interacting convection, rotation and shear flow for specific applications at the present time, however. Before doing so, the traditional laboratory assumptions of our study must first be replaced by more realistic conditions for geophysical situations.

One of us (D.H.H.) was employed by the National Solar Observatory of the National Optical Astronomy Observatories (NOAO) during much of this work. NOAO is operated by the Association of Universities for Research in Astronomy, Inc., under contract AST 78-17292 with the National Science Foundation. We are grateful for their support of this project. The calculations described in this paper were done on the CRAY computers at the National Center for Atmospheric Research (NCAR). We wish to thank NCAR and the Scientific Computing Division for their grant of this machine time. This research was also supported in part by the California Space Institute of the University of California.

REFERENCES

AGEE, E. M. 1984 Observations from space and thermal convection: a historical perspective. *Bull. Am. Met. Soc.* **65**, 938–949.

BRUNT, D. 1951 Experimental cloud formation. *Compendium of Meteorology*, pp. 1255–1262. Boston: American Meteorological Society.

BUSSE, F. H. 1982 Thermal convection in rotating systems. *Proc. 9th US Nat. Cong. Appl. Mech., Am. Soc. Mech. Eng.* pp. 299–305.

BUSSE, F. H. 1983 Generation of mean flows by thermal convection. *Physica* **9D**, 287–299.

CHANDRASEKHAR, S. 1961 *Hydrodynamic and Hydromagnetic Stability*. Clarendon.

CLEVER, R. M. & BUSSE, F. H. 1977 Instabilities of longitudinal convection rolls in an inclined layer. *J. Fluid Mech.* **81**, 107–127.

CLEVER, R. M., BUSSE, F. H. & KELLY, R. E. 1977 Instabilities of longitudinal convection rolls in Couette flow. *Z. angew. Math. Phys.* **28**, 771–783.

DEARDORFF, J. W. 1965 Gravitational instability between horizontal plates with shear. *Phys. Fluids* **8**, 1027–1030.

FLASAR, F. M. & GIERASCH, P. J. 1978 Turbulent convection within rapidly rotating superdiabatic fluids with horizontal temperature gradients. *Geophys. Astrophys. Fluid Dyn.* **10**, 175–212.

HART, J. E. 1971 Transition to a wavy vortex regime in convective flow between inclined plates. *J. Fluid Mech.* **48**, 265–271.

HATHAWAY, D. H. & SOMERVILLE, R. C. J. 1983 Three-dimensional simulations of convection in layers with tilted rotation vectors. *J. Fluid Mech.* **126**, 75–89.

HATHAWAY, D. H., TOOMRE, J. & GILMAN, P. A. 1980 Convective instability when the temperature gradient and rotation vector are oblique to gravity. II. Real fluids with effects of diffusion. *Geophys. Astrophys. Fluid Dyn.* **15**, 7–37.

INGERSOLL, A. P. 1966 Convective instabilities in plane Couette flow. *Phys. Fluids* **9**, 682–689.

KUETTNER, J. P. 1971 Cloud bands in the Earth's atmosphere: observations and theory. *Tellus* **23**, 404–425.

KUO, H. L. 1963 Perturbations of plane Couette flow in stratified fluid and the origin of cloud streets. *Phys. Fluids* **6**, 195–211.

LEMONE, M. A. 1973 The structure and dynamics of horizontal roll vortices in the planetary boundary layer. *J. Atmos. Sci.* **30**, 1077–1091.

LEMONE, M. A. 1983 Momentum transport by a line of cumulonimbus. *J. Atmos. Sci.* **40**, 1815–1834.

LIPPS, F. B. 1971 Two-dimensional numerical experiments in thermal convection with vertical shear. *J. Atmos. Sci.* **28**, 3–19.

SOMERVILLE, R. C. J. 1971 Bénard convection in a rotating fluid. *Geophys. Fluid Dyn.* **2**, 247–262.

SOMERVILLE, R. C. J. & GAL-CHEN, T. 1979 Numerical simulations of convection with mean vertical motion. *J. Atmos. Sci.* **36**, 805–815.

SOMERVILLE, R. C. J. & LIPPS, F. B. 1973 A numerical study in three space dimensions of Bénard convection in a rotating fluid. *J. Atmos. Sci.* **30**, 590–596.

VERONIS, G. 1959 Cellular convection with finite amplitude in a rotating fluid. *J. Fluid Mech.* **5**, 401–435.

WEISS, N. O. 1964 Convection in the presence of constraints. *Phil. Trans. R. Soc. Lond.* A **256**, 99–147.

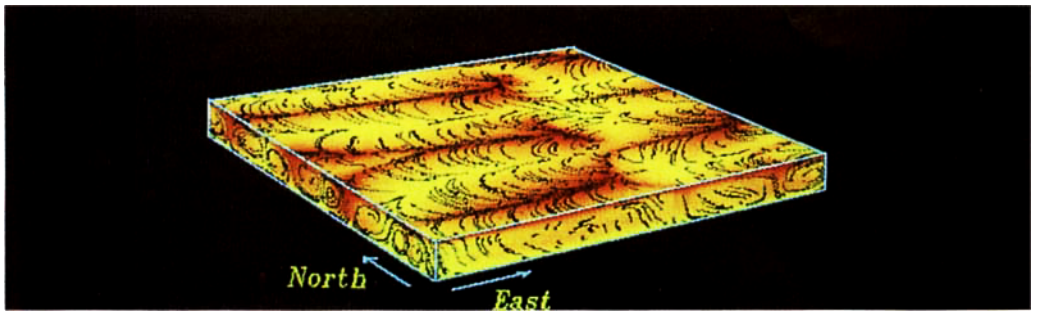

FIGURE 1. A three-dimensional perspective view of the velocity and temperature fields for the non-rotating case with $Re=50$, $Ra=10\,000$, $Pr=1.0$ and $t=1.3$. Colour is used to represent temperature with yellow being hot and red cold. The trajectories of several hundred black markers are plotted on each of the three visible surfaces by marking their previous positions. Here the convective eddies are oriented east to west – in the direction of the imposed shear flow. Both the top and south surfaces show that upward motions carry westward momentum while downward motions carry eastward momentum.

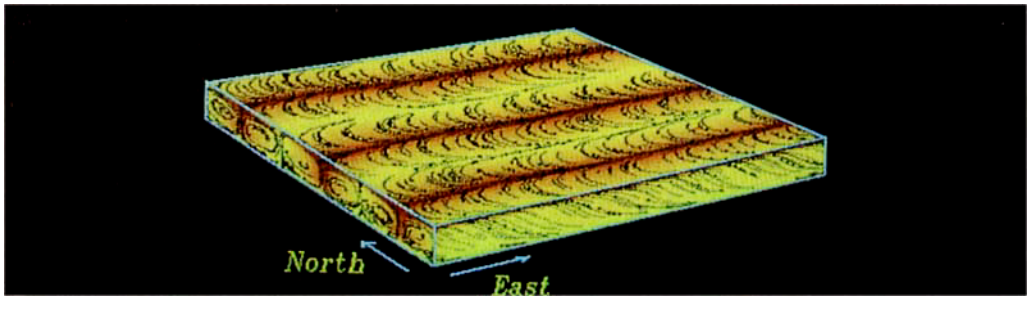

FIGURE 2. A perspective view of the velocity and temperature fields for the non-rotating case with $Re=100$, $Ra=10\,000$, $Pr=1.0$, $t=1.3$. The convection forms a series of broad rolls aligned with the shear flow. The downward momentum flux is seen in the trajectories shown on the top and south surfaces.

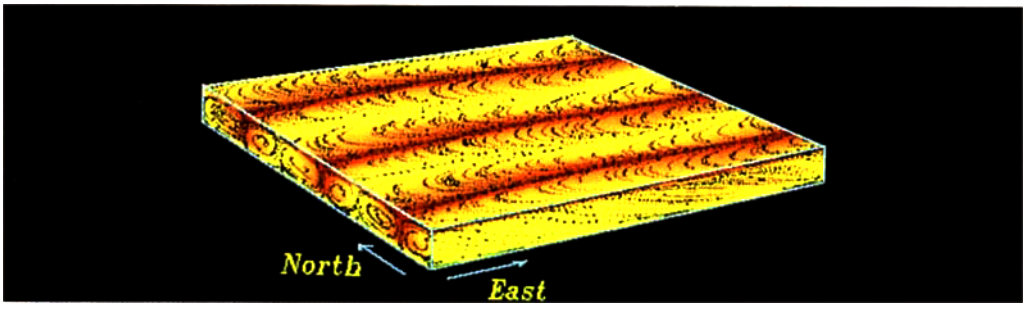

FIGURE 3. A perspective view of the velocity and temperature fields for the non-rotating case with $Re=200$, $Ra=10\,000$, $Pr=1.0$, $t=0.65$. The convection forms a series of broad rolls aligned with the shear flow. The strong downward momentum flux is seen in the trajectories shown on the top and south surfaces.

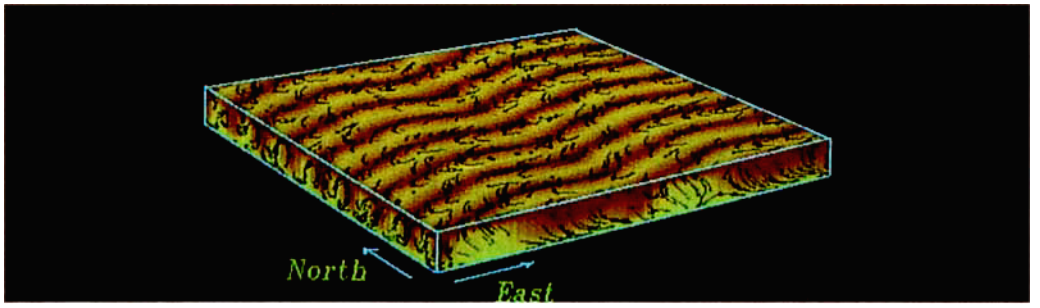

FIGURE 5. A perspective view of the velocity and temperature fields for the rotating case with $Ta=10\,000$, $\phi=90°$, $Re=50$, $Ra=10\,000$, $Pr=1.0$ and $t=1.3$. The convection forms a series of narrow wavy rolls which are nearly aligned with the shear flow. The horizontal motions on the top surface are nearly parallel to the roll axes. The downward flux of eastward momentum is seen in the trajectories shown on the south surface.

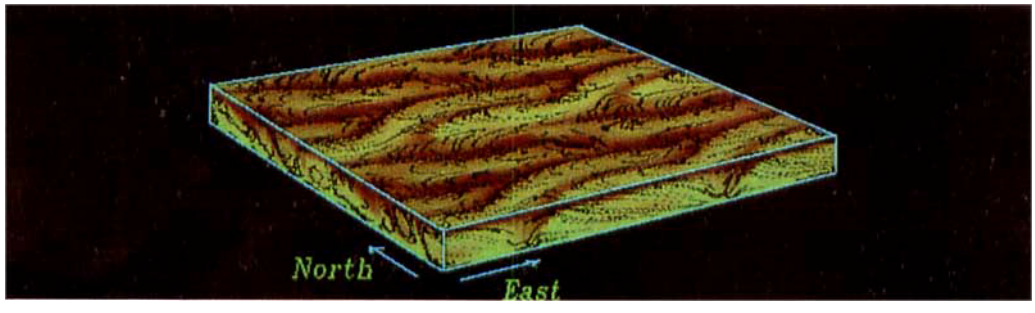

FIGURE 6. A perspective view of the velocity and temperature fields for the rotating case with $Ta=10\,000$, $\phi=90°$, $Re=100$, $Ra=10\,000$, $Pr=1.0$ and $t=1.30$. The convective rolls are somewhat broader but less organized than in the lower-Reynolds-number case.

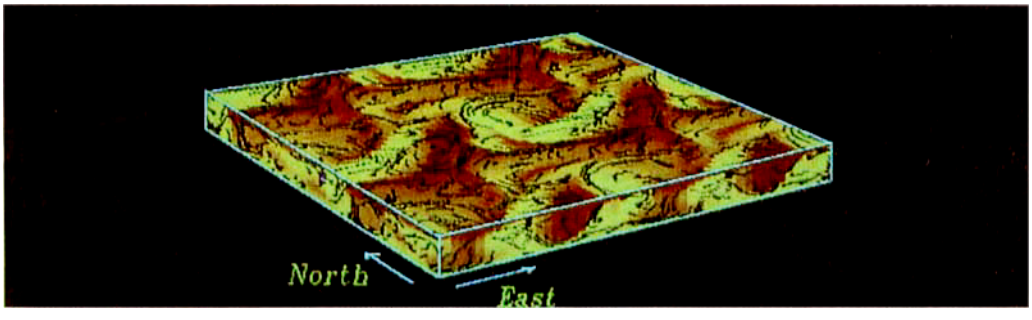

FIGURE 7. A perspective view of the velocity and temperature fields for the rotating case with $Ta=10\,000$, $\phi=90°$, $Re=200$, $Ra=10\,000$, $Pr=1.0$ and $t=0.65$. The convection is more chaotic and exhibits cyclonic and anticyclonic motions on the top surface.

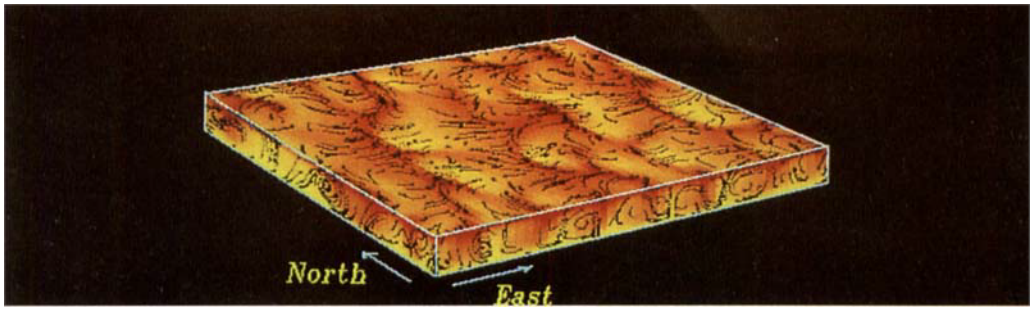

FIGURE 9. A perspective view of the velocity and temperature fields for the rotating case with $Ta=10\,000, \phi=15°$, $Re=+50$, $Ra=10\,000$, $Pr=1.0$ and $t=1.3$. The convection forms eddies which are aligned with the rotation axis instead of the shear flow.

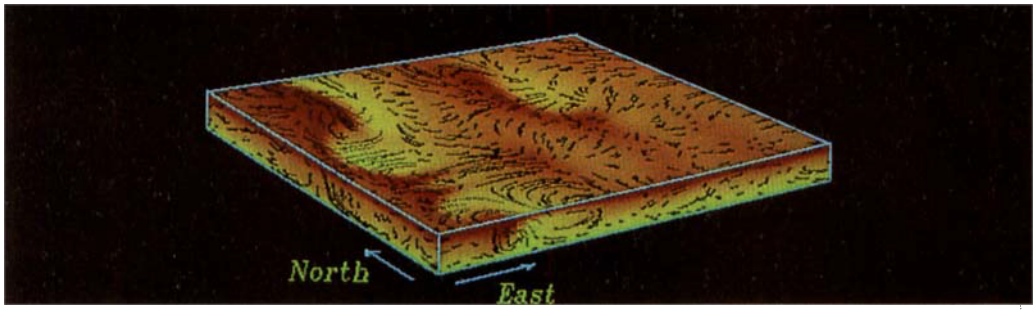

FIGURE 10. A perspective view of the velocity and temperature fields for the rotating case with $Ta=10\,000, \phi=15°$, $Re=+100$, $Ra=10\,000$, $Pr=1.0$ and $t=1.3$. The convection forms broad eddies which are aligned with the rotation axis instead of the shear flow. The convection itself is spatially intermittent and much weaker than in the more weakly sheared case.

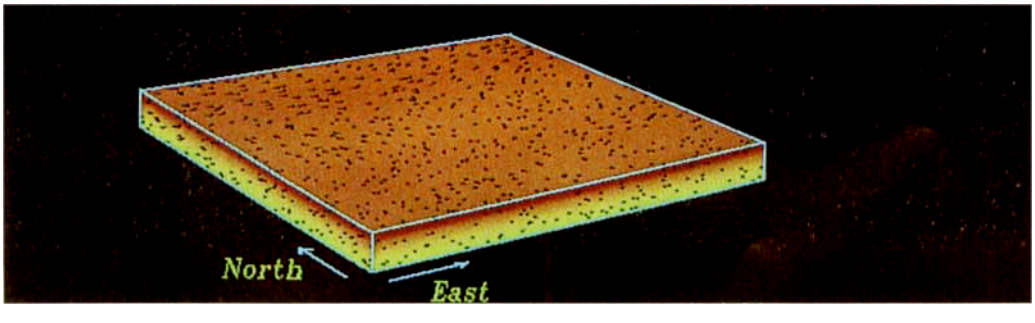

FIGURE 11. A perspective view of the velocity and temperature fields for the rotating case with $Ta=10\,000, \phi=15°$ and $Re=+200$, $Ra=10\,000$, $Pr=1.0$ and $t=0.22$. The convective motions are quenched and the temperature field relaxes to a conductive profile.

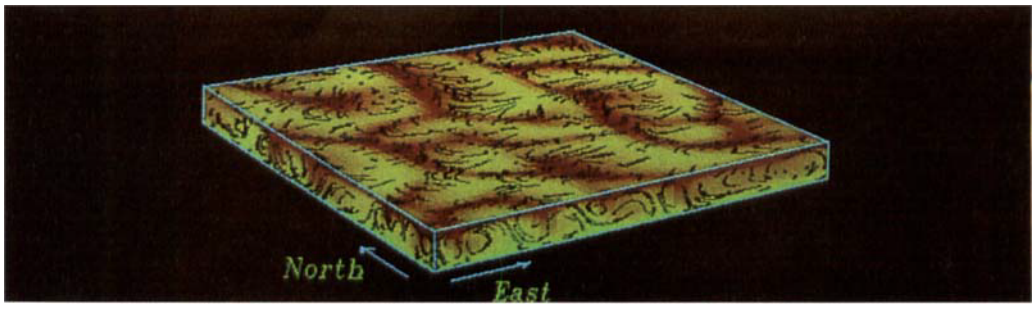

FIGURE 13. A perspective view of the velocity and temperature fields for the rotating case with $Ta=10\,000, \phi=15°$, $Re=-50$, $Ra=10\,000$, $Pr=1.0$ and $t=1.3$. The convection tends to be aligned with the rotation axis but there is some evidence for structures aligned with the shear. The trajectories on the south surface are tilted such that upward flows carry westward momentum. This momentum flux extracts energy and momentum from the eddies and enhances the imposed mean flow.

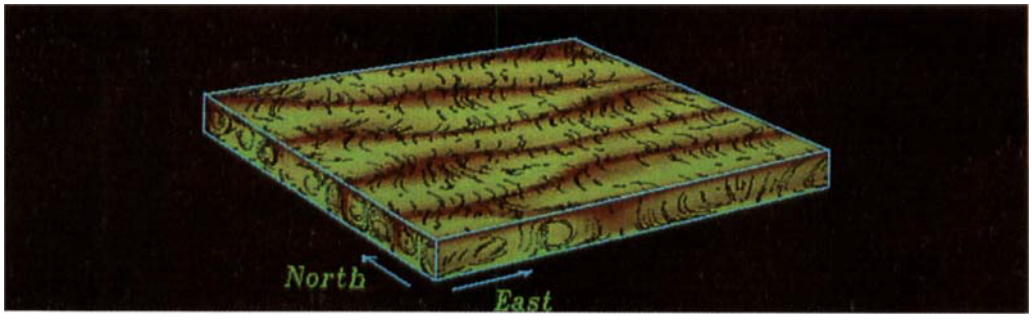

FIGURE 14. A perspective view of the velocity and temperature fields for the rotating case with $Ta=10\,000, \phi=15°$, $Re=-100$, $Ra=10\,000$, $Pr=1.0$ and $t=1.3$. The convection forms rolls which are aligned with the imposed shear flow. There is little evidence for tilted trajectories on either the south or the west surface.

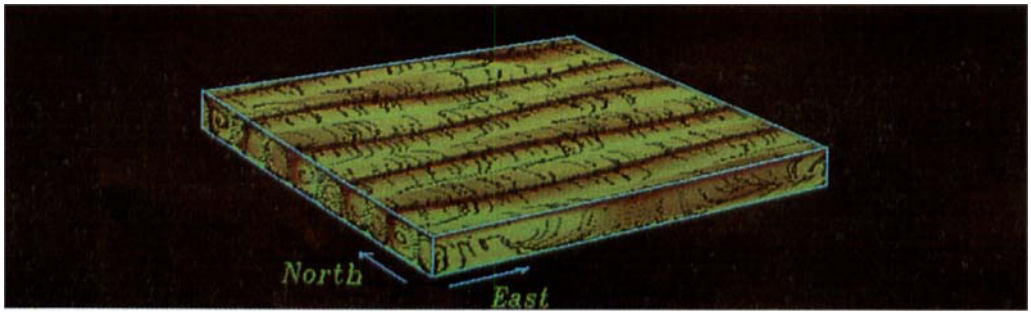

FIGURE 15. A perspective view of the velocity and temperature fields for the rotating case with $Ta=10\,000$, $\phi=15°$, $Re=-200$, $Ra=10\,000$, $Pr=1.0$ and $t=0.65$. The convection forms broad, regular rolls which are aligned with the shear flow. There is little evidence of tilted trajectories on either the south or west surface. However, the trajectories on the top surface show eastward motions in the updrafts and westward motions in the downdrafts.